Microscopy and Microanalysis, **30** (Suppl 1), 2024, 1194–1197
https://doi.org/10.1093/mam/ozae044.595

Microscopy AND Microanalysis

Meeting-report

Corrosion Behavior of a Titanium Nanostructured Surface Fabricated by Glancing Angle Sputter Deposition

Matteo Bertapelle[1], Joel Borges[2,3], Julia Mirza-Rosca[4,5], and Filipe Vaz[2,3,5]

[1]*Department of Information Engineering, University of Padova, Padova, PD, Italia*
[2]*Physics Centre of Minho and Porto Universities (CF-UM-UP), University of Minho, Braga, Portugal*
[3]*LaPMET - Laboratory of Physics for Materials and Emergent Technologies, University of Minho, Braga, Portugal*
[4]*Mechanical Engineering Department, University of Las Palmas de Gran Canaria, Las Palmas de Gran Canaria, Spain*
[5]*Transylvania University of Brasov, Materials Engineering and Welding Department, Brasov, Romania*

*Correspondence author: julia.mirza@ulpgc.es

Introduction

The optical, thermal and electrical properties of thin porous films provide an advantage in the optimization of several devices' performance, allowing them to tailor their response according to the particular requirements of the envisaged application. Furthermore, porous thin films and highly structured growth geometries, characterized by low and graded refractive index (tuned along the film thickness), are highly desirable for optical applications, such as antireflection coatings [1-3] and flexible optical-based sensors [4,5]. The fact is that the effective properties of highly porous materials are determined by the spatial configuration of voids and porosity, namely their size, shape and distribution [6].

To identify the optimal roughness and/or porosity of a thin film surface that can respond more adequately to a given application requirement, several different systems have been optimized, using a wide variety of deposition techniques, configurations and geometries. Glancing Angle Deposition (GLAD) is a promising technique for preparing nanostructured thin films, including metallic or intermetallic, oxides and nitrides, and carbides, among others, using environmentally friendly magnetron sputtering processes. The production of nano-designed thin films using GLAD is an invaluable emerging tool to optimize the material's physicochemical behavior, allowing to tailor the mechanical, electrical, optical, and bioactive properties [7].

This study aimed to investigate how the corrosion behavior of titanium thin films is influenced by sculptured and surface-patterned nanofeatures produced by using special growing geometries. For this, titanium thin films with different nanostructures and approximately the same thickness (0.90 ± 0.01 μm) were prepared, and their corrosion responses were evaluated.

Experimental

Experimental design and deposition conditions

The titanium thin films were prepared by GLAD in a DC magnetron sputtering equipment, using a custom-made deposition system [8]. The two zigzag-like films were prepared by changing the main direction of impinging particles, α, between 20° and 40°, adding the 180° azimuthal rotation (ϕ) to obtain the zigzag-like geometry. A schematic of the deposition system is depicted in Fig. 1 and the details about GLAD geometry and specificities can be found elsewhere [8]. The thin films were grown in an alternate inclined structure (to achieve 2 complete zigzags), varying the inclination angle of the imping particles, α, between 20° and 40° in both directions.

During the depositions, a pure Ti rectangular target (200×100×6 mm^3, 99.99% purity) was sputtered with a current density of 75 A/m^2, using a gas atmosphere composed of pure Ar (flow of 25 sccm, corresponding to a partial pressure of 3.5×10^{-1} Pa). The base pressure was kept below 5×10^{-4} Pa in all depositions. Before the depositions, the substrates were cleaned with ethanol to remove molecular layers of contaminants from the surfaces. To increase the surface energy and the thin films' adhesion, the substrates were plasma-activated [9], using a low-pressure Plasma Cleaner (Diener Electronic Zepto Model, Ebhausen, Germany), equipped with a 13.56 MHz RF generator. The treatments were carried out in a pure Ar atmosphere (0.80 mbar) for 15 min, applying a 50 W power.

The deposition time was adjusted to prepare different the samples with a similar thickness, which was set to be about 0.90 ± 0.01 μm. Glass and silicon (boron doped, p-type, monocrystalline [100] orientation) substrates were used in all depositions, placed in a grounded GLAD substrate holder, Fig. 1.

Characterization

The thickness and microstructural characteristics of the thin films were assessed by Scanning Electron Microscopy (SEM), using a high-resolution microscope (FEI Nova NanoSEM 200). The surface morphology of the films, namely roughness and porosity, was studied by Atomic Force Microscopy (AFM), using a high-resolution Nano-Observer AFM microscope (Concept Scientific Instruments), in resonant mode. Scan sizes of 10×10 μm^2 were carried out in each sample, at a resolution of 1024×1024 px^2 and 1 line/s scan speed.

The specimens were subjected to corrosion testing in simulated body fluid (a Ringer Grifols solution) using a Biologic SP-150 potentiostat. The EIS test was performed by measuring individual sine waves at frequencies ranging from 10^{-1} to 10^5 Hz for both types of samples, following the applicable standard ISO 16773-1-4:2016. Through analysis of the gathered spectra, it was possible to establish a relationship between the chemical and physical characteristics of the synthesized alloys and the continuing electrochemical process.

Results and discussion

Fig. 1 presents the geometrical scheme for the deposition of sputtered species from a target by GLAD. The two analysed samples were named by the inclination growth angle, 20ZZ (prepared with a 20° zigzag architecture, Fig. 1) and 40ZZ (prepared with a 40° zigzag architecture, Fig. 1). The obtained zigzag structures were observed and characterized by SEM. Fig. 2 shows the surface and cross-section features of the films (the last used also to obtain the thickness of the films), together with the surface images of the two samples, obtained by atomic force microscopy (AFM). The root mean square (RMS) roughness obtained by the AFM images analysis was found to be 8 nm for the 20ZZ sample (20° zigzag architecture, Fig. 1), while for the 40ZZ (40° zigzag, Fig. 1) sample, the value was determined to be 15 nm.

To further demonstrate the impact of the deposition angle and the correspondent roughness/porosity evolution in the films' behavior, the corrosion resistance, the electrochemical tests, including corrosion potential vs time, the potentiodynamic polarization and electrochemical impedance spectroscopy (EIS), were performed on the samples.

From Fig. 3a), it can be perceived that while the sample prepared at 20° (sample 20ZZ) achieved a passivation state, while the the sample prepared at 40° (40ZZ) was still corroding after 1 hour of immersion in Ringer solution. Moreover, the observed positive shift in E_{corr} (see Fig. 3b), and the decrease in corrosion current, provided additional evidence supporting the improved corrosion resistance of the sample prepared at a 20° zigzag structure. This shows a significant effect of the surface features on the films behavior, providing further evidence on the importance of the GLAD geometry to obtain materials with tailored response.

The EIS spectra measured for the two samples are presented as Nyquist complex plane plots in Fig. 4. The spectrum of sample 20ZZ (20° zigzag geometry, Fig. 1) is characterized by a single constant time (visualized by a capacitive loop discerned for the passive film), which can be associated with a parallel RC connection [10] in the electrical equivalent circuit. Two well-separated time constants can be observed in the spectrum of the 40ZZ (40° zigzag geometry, Fig. 1) sample; there is a linear region in the low-frequency end of the spectrum suggesting that diffusion might play a crucial part in the corrosion process [11]. This, combined with the relatively low impedance magnitude measured for this sample, might imply that the thin film was more porous (rougher surfaces as actually demonstrated by the AFM results) in this case and offered less diffusional resistance.

Conclusions

The results from this work show that it is possible to tailor the surface characteristics of a thin film by simply varying the angle of the deposition. As the angle of deposition increases, the corrosion resistance decreases due to the shadow effect of the growing process that increases the porosity/roughness of the film and hence the active surface area.

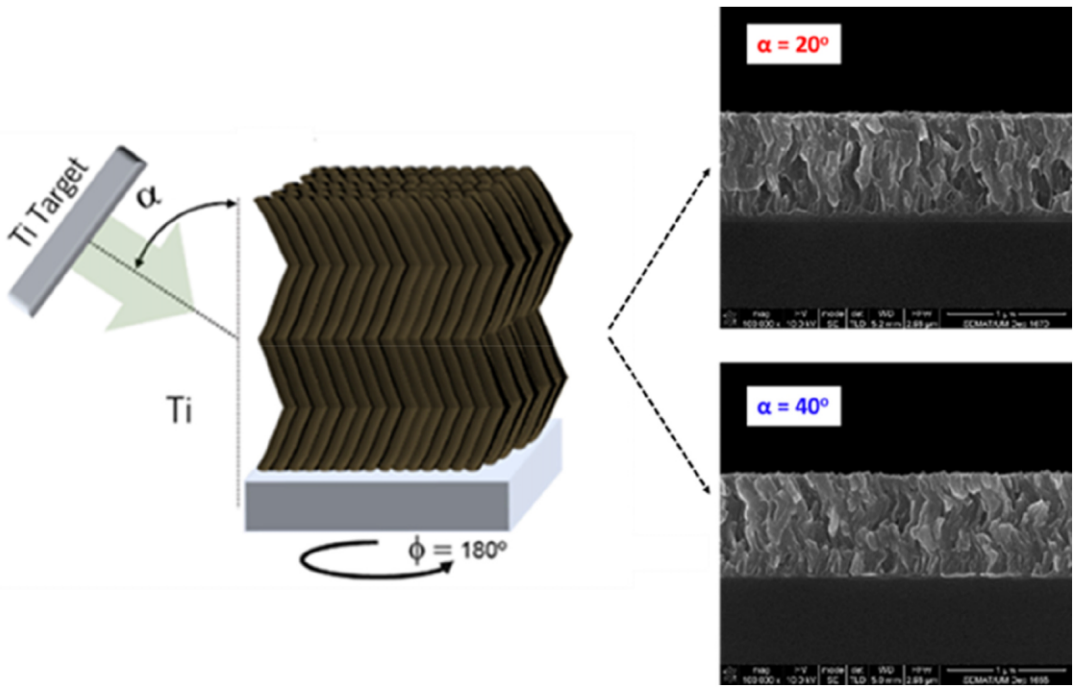

Fig. 1. Geometry of the GLAD method used for the preparation of the Ti thin films and SEM micrographs obtained is cross-sectional view.

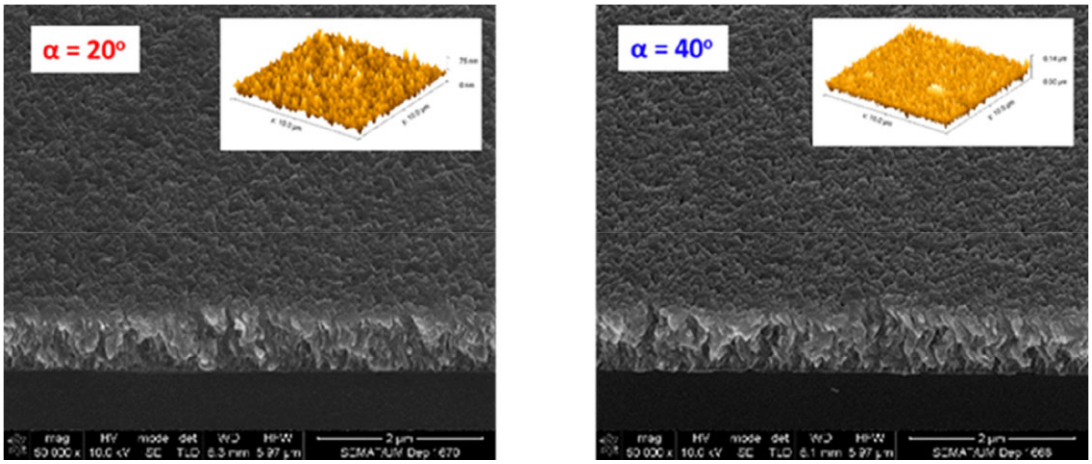

Fig. 2. SEM micrographs, observed in tilted anggles, and AFM images of the film's surface.

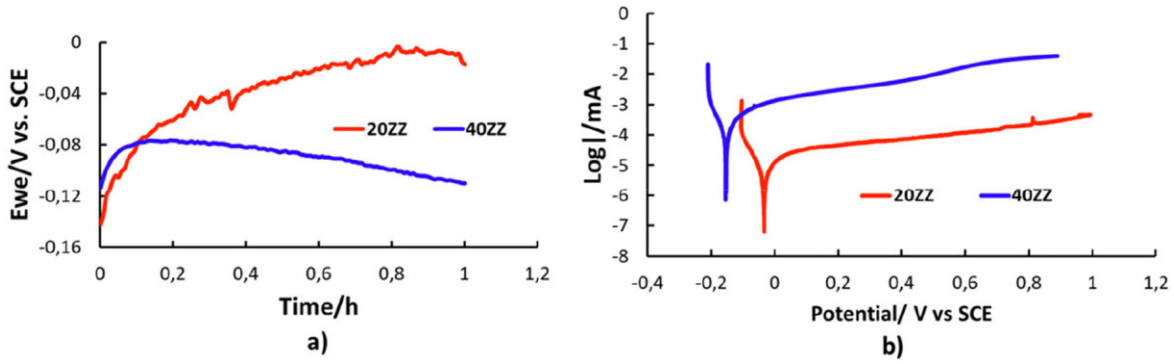

Fig. 3. a) Open circuit potential vs time for both samples during immersion time. b) Potentiodynamic polarization curves of the samples in Ringer solution.

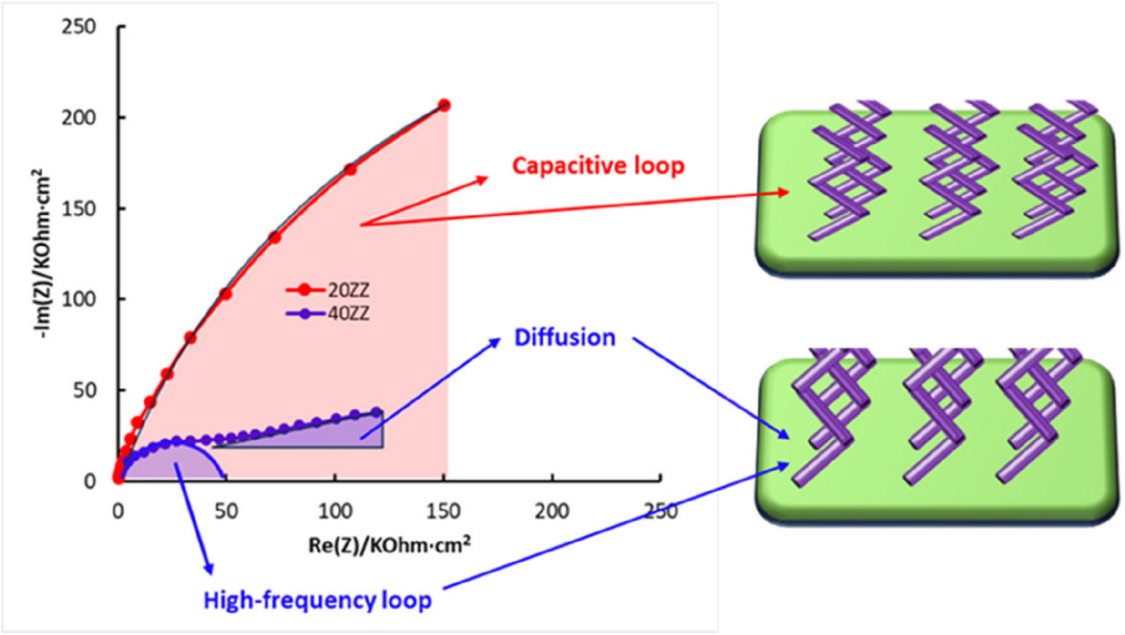

Fig. 4. Nyquist plots for the samples immersed in Ringer solution.

References

1. K. Katagiri *et.al*, *Polym. J.* **47** (2015) 190–194. https://doi.org/10.1038/pj.2014.104.
2. S.R. Kennedy, M.J. Brett, *Appl. Opt.* **42** (2003) 4573. https://doi.org/10.1364/AO.42.004573.
3. T. Chaikeeree *et al.*, *Opt. Mater. (Amst)*. **121** (2021) 111545, https://doi.org/10.1016/j.optmat.2021.111545.
4. P. Girault *et al.*, *Opt. Mater. (Amst)*. **72** (2017) 596–601, https://doi.org/10.1016/j.optmat.2017.07.005.
5. M.S. Rodrigues *et al.*, *Appl. Sci.* **11** (2021) 5388. https://doi.org/10.3390/app11125388.
6. N. Shpigel *et.al.*, *Nat. Commun.* **10** (2019) 4394. https://doi.org/10.1038/s41467-019-12277-4.
7. A. Barranco *et al.*, *Prog. Mater. Sci.* **76** (2016) 59–153. https://doi.org/10.1016/j.pmatsci.2015.06.003.
8. M.S. Rodrigues *et al.*, *Nanotechnology* **30** (2019), 225701, https://doi.org/10.1088/1361-6528/ab068er.
9. P. Pedrosa *et al.*, *Plasma Process. Polym.* **13** (2016) 341–354, https://doi.org/10.1002/ppap.201500063.
10. Vasilescu, *et al.*, *Materials and Corrosion*, **51** (2002): 413-417. https://doi.org/10.1002/1521-4176(200006)51:6<413::AID-MACO413>3.0.CO;2-3
11. Jimenez-Marcos C. *et al.*, *Bioengineering*. 2022; **9**(11):686. https://doi.org/10.3390/bioengineering9110686